Isostructural rare-earth metal-organic frameworks for enhanced MTO product separation and efficient methane storage

Guo-Tong Du,[a] Xin-Ai Guo,*[a] Teng-Long Liu,[a] Hong-Xin Li,[b] Ya-Nan Ma,[a] Dong-Xu Xue*[a]

[a]Shaanxi Key Laboratory of New Concept Sensors and Molecular Materials, Key Laboratory of Applied Surface and Colloid Chemistry of Ministry of Education, School of Chemistry & Chemical Engineering, Shaanxi Normal University, Xi'an 710119, P. R. China

[b]Shaanxi Key Laboratory of Low Metamorphic Coal Clean Utilization, School of Chemistry and Chemical Engineering, Yulin University, Yulin, 719000, P. R. China

E-mail: xuedx@snnu.edu.cn; guoxa@snnu.edu.cn

Table of Contents

1. Materials and General Procedures

All reagents were obtained from commercial sources and used without further purification. The organic linker 2,2'-bipyridine-5,5'-dicarboxylic acid (H_2BPyDC) were purchased from Bide Pharmatech Ltd. $Yb(NO_3)_3 \cdot 6H_2O$ and $Y(NO_3)_3 \cdot 6H_2O$ were purchased from Macklin; N, N dimethylformamide (DMF), acetone, 2-FBA (FBA = 2-fluorobenzoic acid) , ethyl alcohol were purchased from Sinopharm.

PXRD measurements were performed on a Bruker D8 Advance diffractometer with Cu *K*α (λ = 1.5418 Å), and the X-ray tube was operated at 40 kV and 40 mA. Thermogravimetric analysis (TGA) was performed under a continuous N_2 flow and recorded on a Q600SDT thermal analyzer with a heating rate of 5 °C min^{-1}. Elemental analyses (C, H, and N) were obtained from a Vario EL cube analyzer. Fourier transform infrared (FT-IR) spectrum (400-4000 cm^{-1}, KBr pellet) was collected in the solid state on a Bruker Tensor 27 FT-IR spectrometer.

Synthesis of fcu**-BPyDC-Yb**

A mixture of $Yb(NO_3)_3 \cdot 6H_2O$ (11.68 mg, 0.02175 mmol), H_2BPyDC (10.62 mg，0.02175 mmol), DMF (2.25 mL), 2-FBA (FBA = 2-fluorobenzoic acid, 0.8 mL, 3.48 M/DMF) ethanol (180 μL) were combined in a 20 mL scintillation vial and transferred to an autoclave and heated at 115 °C for 12 h.[1] The colorless polyhedral crystals were collected and washed several times by DMF. Yield ≈ 58.8% (based on H_2BPyDC). Selected IR (KBr, cm^{-1}): 3100(vs), 2379(m), 1658(m), 1598(s), 1580(m), 1571(s), 1422(m), 1380(s), 1363(m), 1336(m), 1138(m), 1024(m), 850(m), 772(m), 694(w), 556(w), 508(vw), 416(vw).

Synthesis of fcu**-BPyDC-Y**

A mixture of $Y(NO_3)_3 \cdot 6H_2O$ (9.58 mg, 0.02175 mmol), H_2BPyDC (10.62 mg，0.02175 mmol), DMF (2.25 mL), 2-FBA (FBA = 2-fluorobenzoic acid, 0.9 mL, 3.48 M/DMF) ethanol (220 μL) were combined in a 20 mL scintillation vial and transferred to an autoclave and heated at 115 °C for 18 h. The colorless polyhedral crystals were collected and washed several times by DMF. Yield ≈ 66.8% (based on H_2BPyDC). Selected IR (KBr, cm^{-1}): 3082(vs), 2380(m), 1649(m), 1589(m), 1538(s), 1428(m), 1381(s), 1363(m), 1328(m), 1118(m), 1028(m), 866(m), 781(m), 695(w), 573(w), 501(vw), 408(vw).

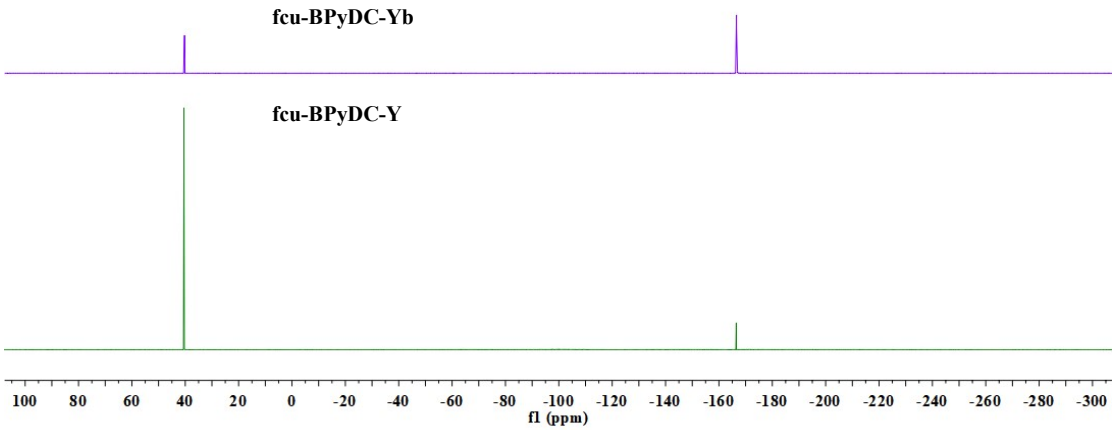

Fig. S1 The ^{19}F NMR (400 MHz, DMSO-d_6) spectra of **fcu**-BPyDC-Yb, **fcu**-BPyDC-Y For all materials, there is a peak at δ = -166 ppm, this signal is attributed to HF, from the dissolved materials in H_2SO_4 and DMSO-d_6.

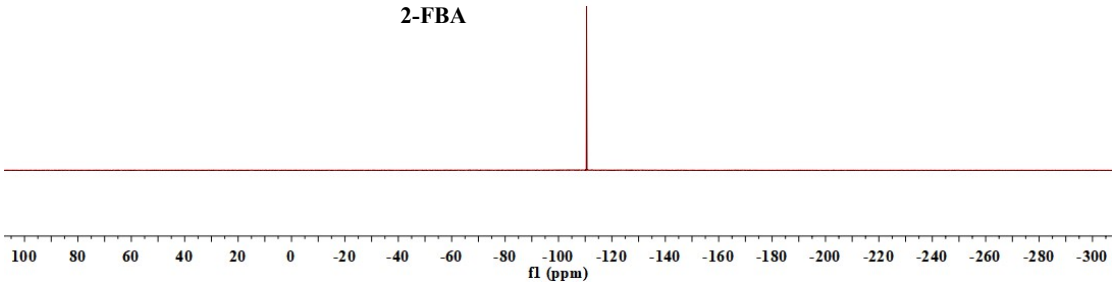

Fig. S2 The ^{19}F NMR (400 MHz, DMSO-d_6) spectra of 2-fluorobenzoic acid, it has a peak at δ = -110 ppm.

2. Powder X-ray Diffraction (PXRD) Patterns

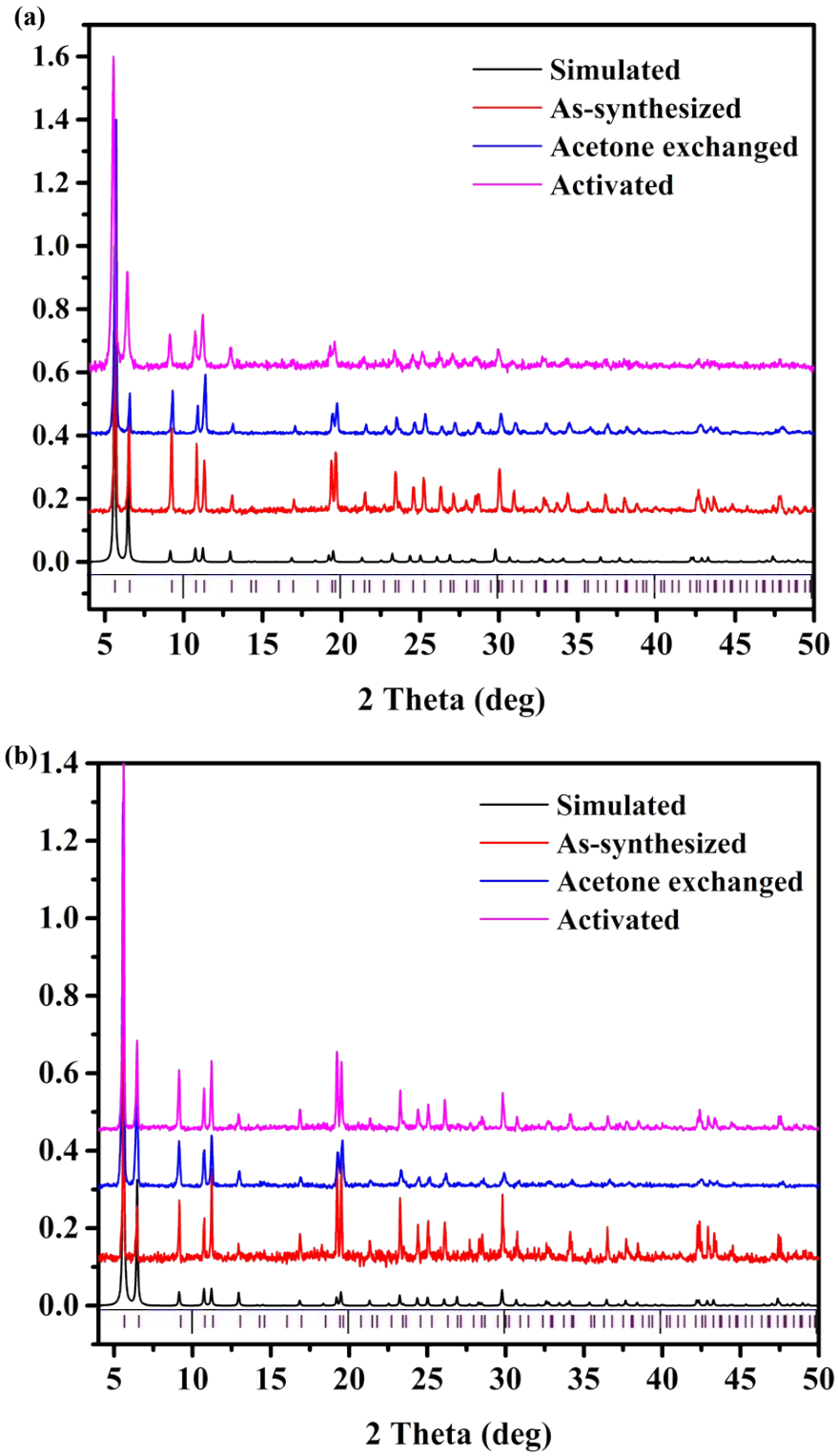

Fig. S3 Powder X-ray diffraction patterns of (a) **fcu**-BPyDC-Yb, (b) **fcu**-BPyDC-Y.

3.Thermal Gravimetric Analysis (TGA)

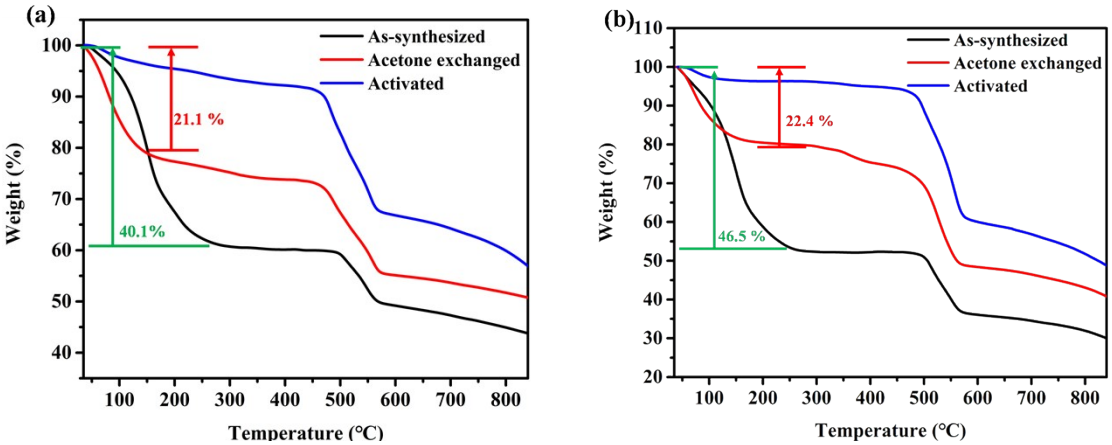

Fig. S4 TGA plots of (a) **fcu**-BPyDC-Yb and (b) **fcu**-BPyDC-Y.

As shown in Figure S4, each of our thermogravimetric data was tested under different conditions and finally summarized together. The green arrow indicates the loss of water and DMF in the original synthesized sample framework; The red color is speculated to indicate the weight loss of acetone solvent in the sample after acetone exchange. These data can roughly match the solvent data calculated based on the crystal structure.

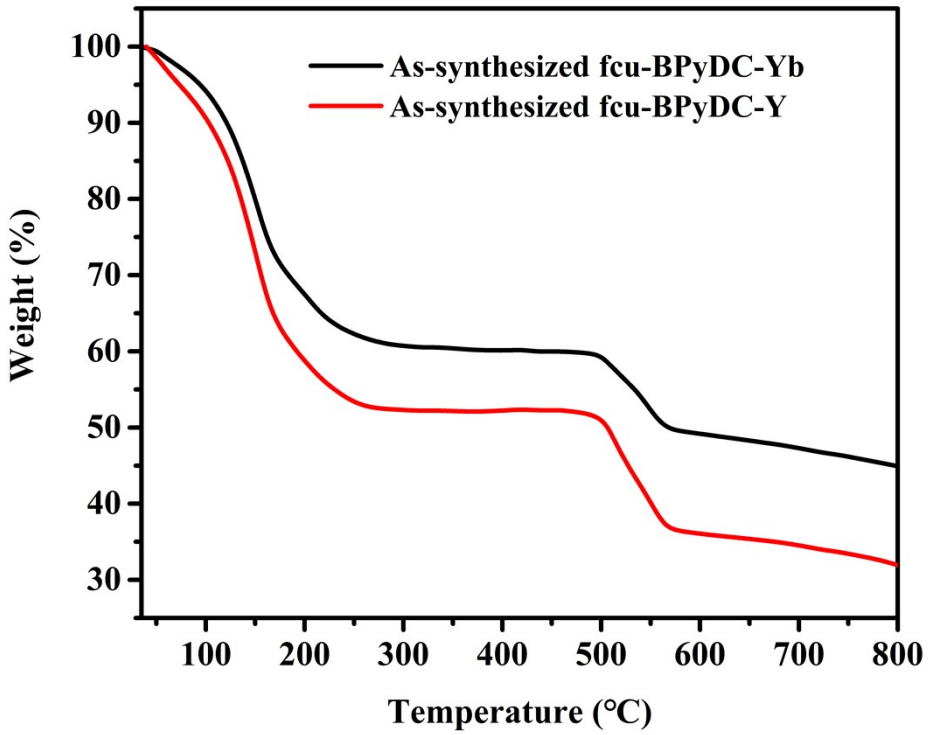

Fig. S5 Overlayed TGA plots of as-synthesized **fcu**-BPyDC-Yb (black) and **fcu**-BPyDC-Y (red).

4. Low-pressure Gas Sorption Measurements

Low-pressure gases sorption isotherms were performed on Quantachrome Instruments automated gas sorption analyzer at relative pressures up to 1 bar. The cryogenic temperature was controlled using liquid nitrogen at 77 K. The bath temperature for the C_2H_4 and C_3H_6 sorption measurements was controlled using a recirculating bath containing an ethylene glycol/H_2O mixture. The apparent surface areas were determined from the nitrogen adsorption isotherms collected at 77 K by applying the BET models.

Sample activation

The as-synthesized sample of **fcu**-BPyDC-Yb and **fcu**-BPyDC-Y were exchanged with acetone at room temperature for one day with refreshing once 8 hours, and then further activated by heating at 120 °C for 12 hours in vacuo.

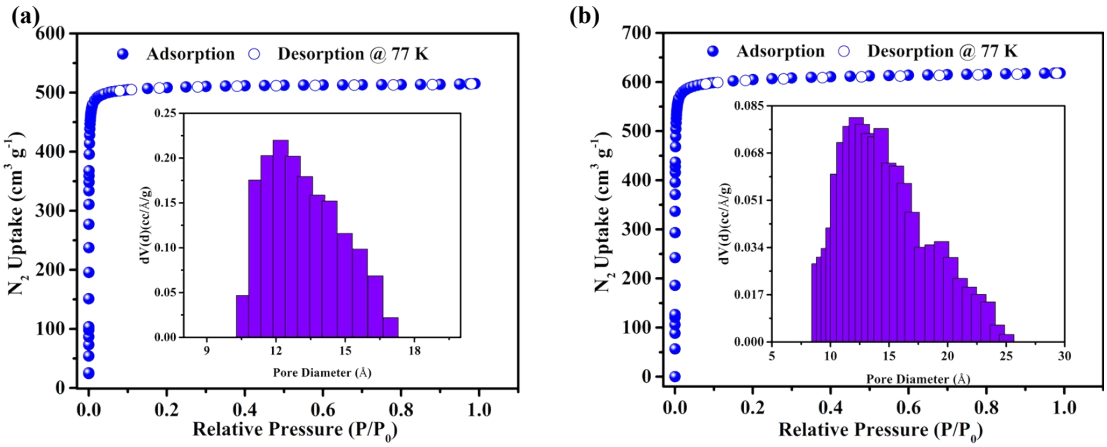

Fig. S6 N_2 sorption isotherms for (a) **fcu**-BPyDC-Yb and (b) **fcu**-BPyDC-Y at 77 K.

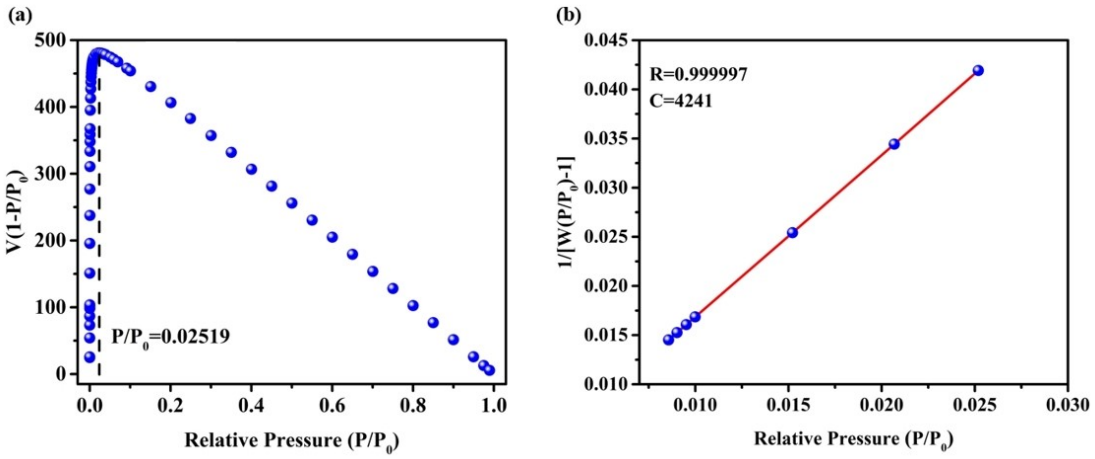

Fig. S7 (a) $V(1-P/P_0)$ vs. P/P_0 for **fcu**-BPyDC-Yb. Only the range below P/P_0 = 0.02519 satisfies the first consistency criterion for applying the BET theory and (b) plot of the linear region for the BET equation.

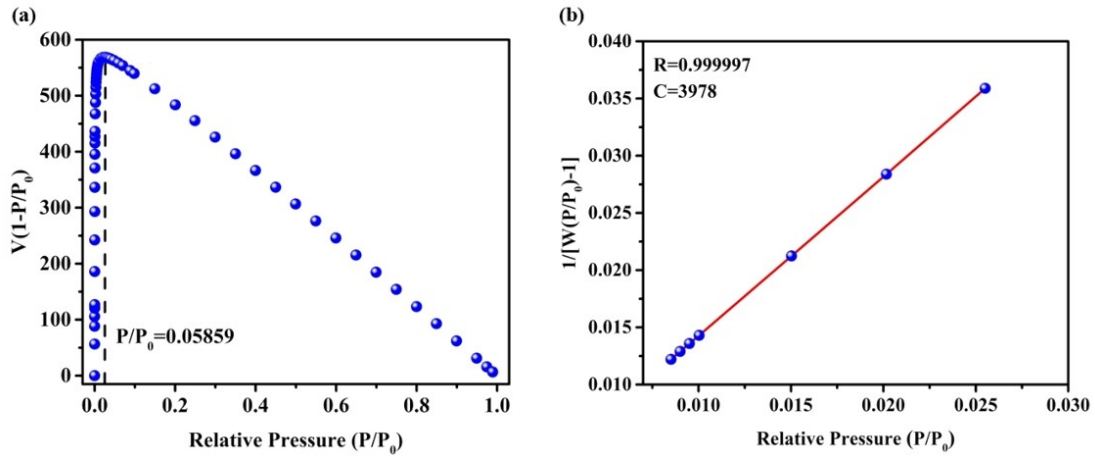

Fig. S8 (a) $V(1-P/P_0)$ vs. P/P_0 for **fcu**-BPyDC-Y. Only the range below P/P_0 = 0.05859 satisfies the first consistency criterion for applying the BET theory and (b) plot of the linear region for the BET equation.

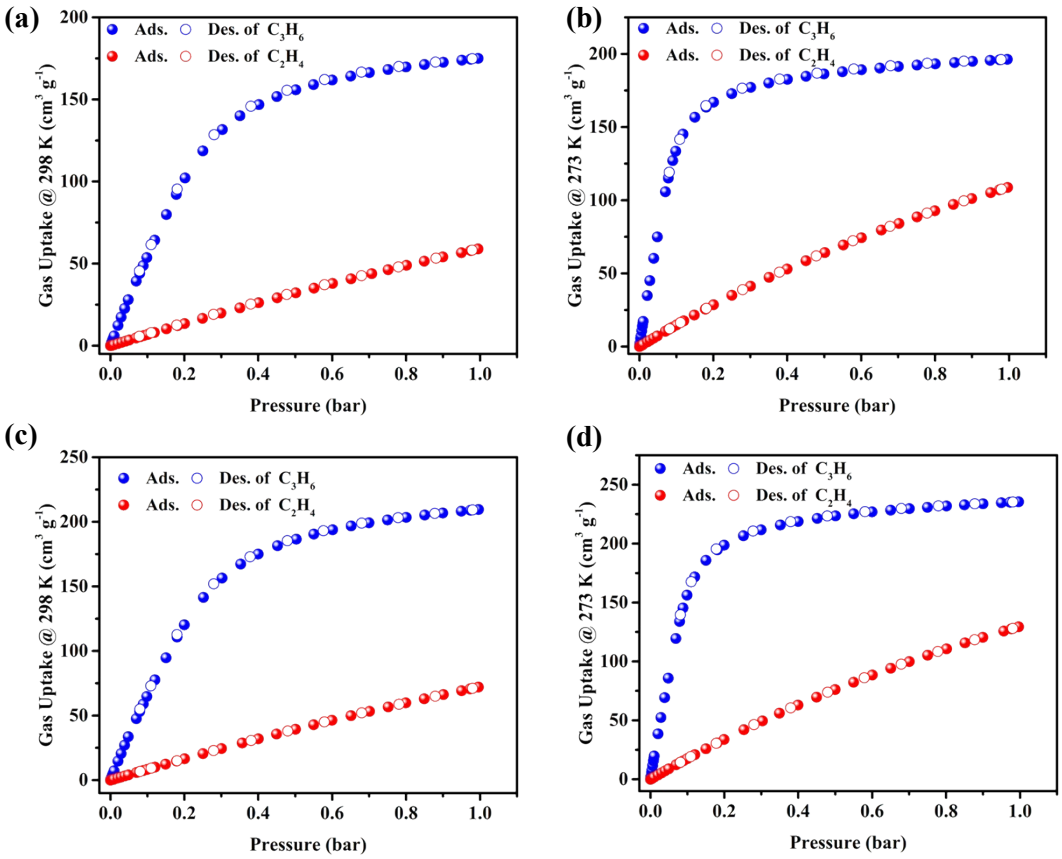

Fig. S9 C_2H_4, C_3H_6 sorption isotherms measured at 298 K and 273 K for **fcu**-BPyDC-Yb (a-b) and **fcu**-BPyDC-Y(c-d), respectively.

5. Calculations of Isosteric Heats of Adsorption (Q_{st})

A virial-type expression comprising the temperature-independent parameters a_i and b_i was employed to calculate the enthalpies of adsorption for C_2H_4 and C_3H_6 (at 273 K and 298 K). In each case, the data were fitted using the equation (Eqn (1)):

$$\ln P = \ln N + \frac{1}{T}\sum_{i=0}^{m} a_i N^i + \sum_{i=0}^{n} b_i N^i \quad (1)$$

Here, P is the pressure expressed in Pa, N is the amount adsorbed in mmol g^{-1}, T is the temperature in K, a_i and b_i are virial coefficients, and m, n represents the number of coefficients required to adequately describe the isotherms. m and n were gradually increased until the contribution of extra added a and b coefficients was deemed to be statistically insignificant towards the overall fit, as determined using the average value of the squared deviations from the experimental values was minimized. The values of the virial coefficients a_0 through a_m were then used to calculate the isosteric heat of adsorption using the following expression (Eqn (2)):

$$Q_{st} = -R\sum_{i=0}^{m} a_i N^i \quad (2)$$

Q_{st} is the coverage-dependent isosteric heats of adsorption and R is the universal gas constant (8.314 J mol^{-1} K^{-1}).

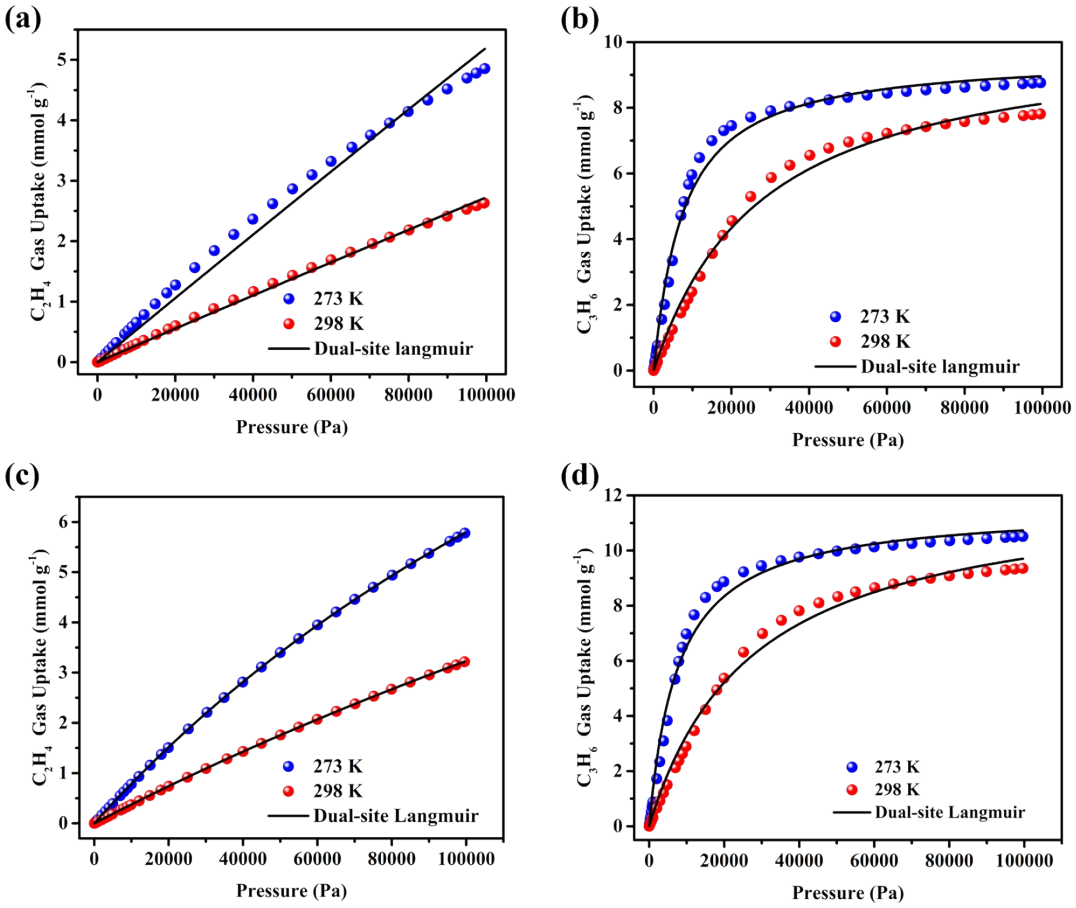

Fig. S10 C_2H_4 and C_3H_6 adsorption isotherms for **fcu**-BPyDC-Yb (a-b) and **fcu**-BPyDC-Y (c-d) were fitted by dual-site Langmuir model at 298 K and 273 K, respectively.

Table S1. The obtained dual-site Langmuir method fitting parameters for C_2H_4 and C_3H_6 adsorption isotherms of **fcu**-BPyDC-Yb.

fcu-BPyDC-Yb	C_2H_4		C_3H_6	
T	**298 K**	**273 K**	**298 K**	**273 K**
b_1	1.77188E-7	2.15357E-7	4.25710E-5	1.58492E-4
b_2	1.77188E-7	2.15357E-7	5.19710E-5	3.36584E-4
Q_1	78.27453	123.38307	18.62937	12.07859
Q_2	78.27453	123.38307	-8.29682	-2.46902
Reduced Chi-Sqr	0.00138	0.02455	0.05210	0.08897
R^2	0.99839	0.99191	0.99495	0.99232

Table S2. The obtained dual-site Langmuir method fitting parameters for C_2H_4 and C_3H_6 adsorption isotherms of **fcu**-BPyDC-Y.

fcu-BPyDC-Y	C_2H_4		C_3H_6	
T	**298 K**	**273 K**	**298 K**	**273 K**
b_1	1.77188E-7	2.15357E-7	3.63521E-5	1.29165E-4
b_2	1.77188E-7	2.15357E-7	3.635243E-5	1.29165E-4
Q_1	78.27453	123.38307	6.19127	5.78249
Q_2	78.27453	123.38307	6.19127	5.78249
Reduced Chi-Sqr	0.00138	0.02455	0.0764	0.15701
R^2	0.99839	0.99171	0.99509	0.99122

6. Selectivity via Ideal Adsorption Solution Theory

IAST (Ideal Adsorption Solution Theory) was used to predict binary mixture adsorption from the experimental pure gas isotherms.[2-4] In order to perform the integrations required by IAST, the single-component C_2H_4 and C_3H_6 adsorption isotherms were first fit to a Dual site Langmuir–Freundlich (DSLF) model as below (Eqn (3)):

$$q = \frac{q_{m,1} b_1 P^{1/n1}}{1 + b_1 P^{1/n1}} + \frac{q_{m,2} b_2 P^{1/n2}}{1 + b_2 P^{1/n2}} \quad \textbf{(3)}$$

Herein, P is the pressure of the bulk gas at equilibrium with the adsorbed phase (kPa), q is the adsorbed amount per mass of adsorbent (mmol g^{-1}), $q_{m,1}$ and $q_{m,2}$ are the saturation capacities of sites 1 and 2 (mmol g^{-1}), b_1 and b_2 are the affinity coefficients of sites 1 and 2 (1/kPa), and n_1 and n_2 represent the deviations from an ideal homogeneous surface. The fitting parameters are shown in Table S1 and S2. Using the pure component isotherm fits, the adsorption selectivity is defined by (eqn (4)):

$$S_{ads} = \frac{q_1 / q_2}{p_1 / p_2} \quad \textbf{(4)}$$

Where q_i is the mole fractions of component i in the adsorbed and bulk phases and p_i is the partial pressure of i in the mixture.

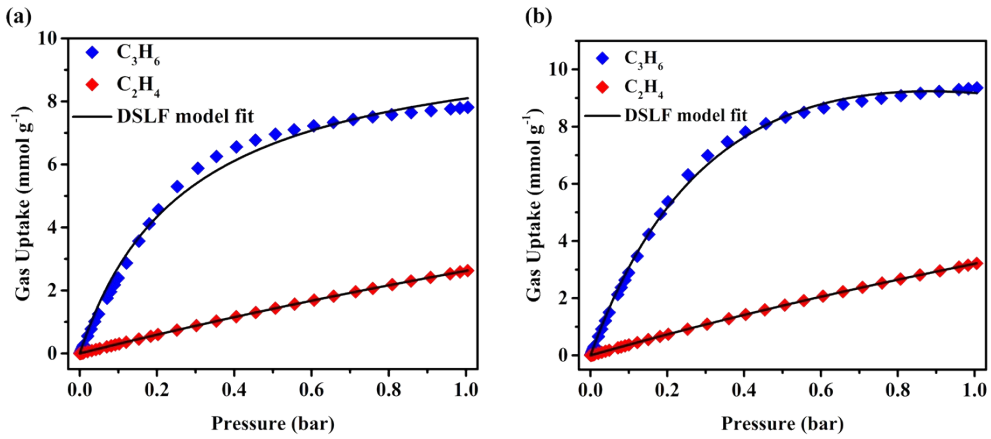

Fig. S11 Dual-site Langmuir–Freundlich fits (lines) of C_2H_4 and C_3H_6 adsorption isotherms (points) measured at 298 K for **fcu**-BPyDC-Yb and **fcu**-BPyDC-Y, respectively.

Table S3. The obtained dual-site Langmuir-Frenudlich fitting parameters for C_2H_4 and C_3H_6 adsorption isotherms of **fcu**-BPyDC-Yb and **fcu**-BPyDC-Y.

	fcu-BPyDC-Yb		**fcu**-BPyDC-Y	
MOFs				
Gas	**C_2H_4**	**C_3H_6**	**C_2H_4**	**C_3H_6**
q_{m1}	0.17289	2.09684	15.76866	2.54721
q_{m2}	11.85326	6.66002	0.06995	7.90976
b_1	4.65E-02	4.34E-05	1.92E-03	7.03E-05
b_2	1.55E-03	4.10E-02	6.31E-02	4.12E-02
$1/n_1$	1.11809	3.73784	1.05627	3.17640
$1/n_2$	1.11441	1.08299	1.15106	1.08808
Reduced Chi-Sqr	1.06988E-5	0.05848	9.75717E-6	0.01960
R^2	0.99999	0.99418	0.99999	0.99864

7. Breakthrough Test

The breakthrough experiments were carried out in homemade HPMC41 gas separation test system (Nanjing Hope Analytical Equipment Co., Ltd). The flow rates of all gases are regulated by mass flow controllers, and the effluent gas stream from the column is monitored by a gas chromatography (GC). In a typical experiment for **fcu**-BPyDC-Yb/Y, approximately 885/588 mg of porous sorbent was ground and packed into a stainless-steel column (25 cm in length × 0.40 cm in internal diameter), with silica wool filling the void space. The sorbent was activated in situ in the column before the temperature of the column was decreased to 298 K. The packed column was initially purged with helium gas for 30 min until no other gases were detected in the effluent.

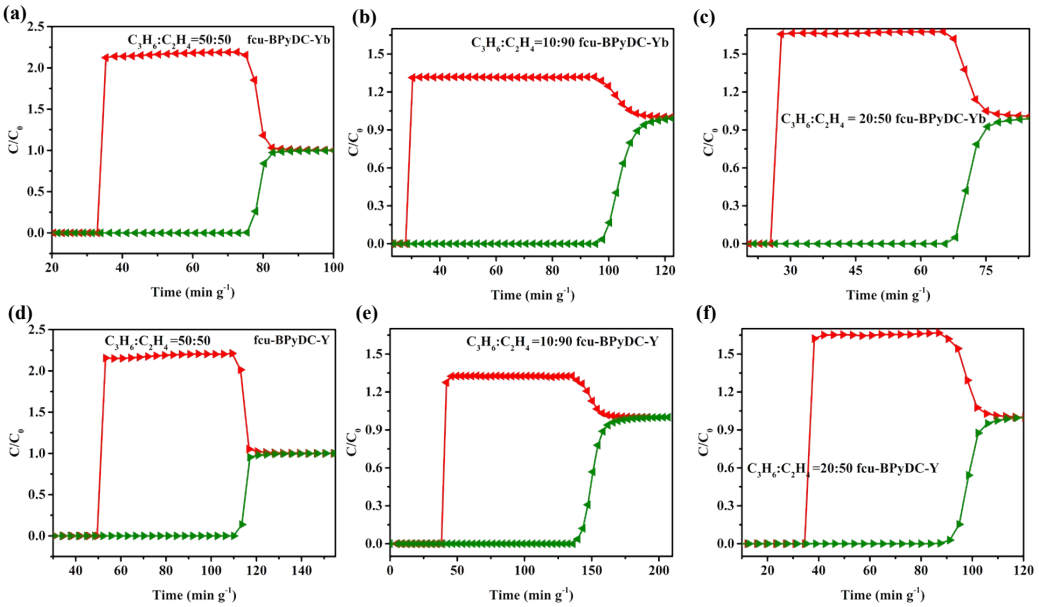

Fig. S12 Experimental column breakthrough curves for C_2H_4/C_3H_6 (50:50) mixture with a total flow of (a) and (d) 2 mL min^{-1} and C_2H_4/C_3H_6 (90:10) mixture with a total flow of (b) and (e) 3 mL min^{-1} and C_2H_4/C_3H_6/He (50:20:30) mixture with a total flow of (c) and (f) 4 mL min^{-1} in an absorber bed packed with **fcu**-BPyDC-Yb/**fcu**-BPyDC-Y at 298 K and 1 bar, respectively.

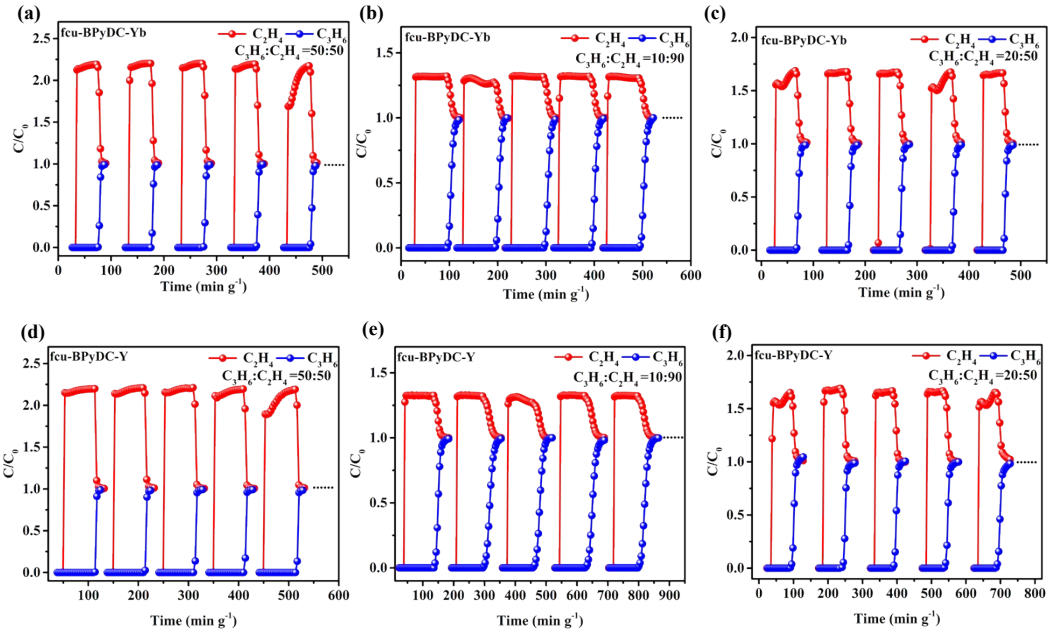

Fig. S13 Cycling breakthrough curves for C_2H_4/C_3H_6 (50:50) mixture with a total flow of (a) and (d) 2 mL min^{-1} and C_2H_4/C_3H_6 (90:10) mixture with a total flow of (b) and (e) 3 mL min^{-1} and C_2H_4/C_3H_6/He (50:20:30) mixture with a total flow of (c) and (f) 4 mL min^{-1} in an absorber bed packed with **fcu**-BPyDC-Yb/**fcu**-BPyDC-Y at 298 K and 1 bar, respectively.

Table S4 Comparison of the $C_2H_4$and C_3H_6 adsorption capacity, selectivity, Q_{st} and breakthrough time for some selected materials.

Porous Material	Gas Uptake ($cm^3 g^{-1}$) (1 bar)		Gas Uptake ($cm^3 g^{-1}$) (0.2 bar)	Gas Uptake ($cm^3 g^{-1}$) (0.5 bar)	Q_{st} (kJ mol^{-1})		IAST Selectivity	Ref
	C_2H_4	C_3H_6	C_3H_6	C_3H_6	C_2H_4	C_3H_6	50/50	
[a]Mn-dtzip	76.7	216.4	116	186.4	24.2	32.3	8.6	5
[a]UPC-33	31.1	94.3	71.7	35.1	10.31	48.96	5.7	6
[a]spe-MOF	48.9	236.9	67.8	160.2	22.5	29.8	7.7	7
[a]LIFM-38	20.0	58.0	26.3	45	27.3	28.1	6.4	8
[a]NEM-7-Cu	63.9	68.3	43.6	62.7	22.5	36.9	8.54	9
[b]NEM-4	164.1	197.4	142	164	35.9	44.5	5.66	10
[a]MFM-202a	64.96	160.8	102	136.2	18	33	8.4	11
[a]iso-MOF-4	73.1	254.5	115.5	203.2	25.4	30.9	7.74	12
[a]HKUST-1	102.1	175	157.7	167.3	45.1	48.5	5.8	13
[a]Mg-MOF-74	165.9	203.2	151.8	195.3	/	/	4.7	14
[a]PCP-1	56.6	70.6	45.2	56.4	25.3	15.8	3.6	15
[a]$Cd_2(AzDC)_2(TPT)_2$	44.9	59.8	33.8	50.7	31	42	1.2	16
[a]Cr-SO_3Ag	63.9	105.8	54.7	78.1	120	101	4.8	17
[a]MAC-4	83.0	127.0	97.2	110.2	17.1	25.3	8.4	18
[a]Zn-BPZ-SA	63.9	68.3	5.5	61.6	23.13	33.65	4.8	19
[a]Zn-BPZ-TATB	91.8	114.0	91.6	106.1	18.4	29.7	7.4	20
[a]$Zn_2(oba)_2(dmim)$	48.3	76.0	60.1	69.7	25.8	33.3	15.6	21
[a]$Cu_3(Me_2BPZ)_2$	52.0	138.0	76.7	118.4	20.68	30.3	7.4	22
[a]$Fe_2Mn(\mu_3\text{-}O)(L)_2$	94.9	291.1	118.7	240	35.8	39.9	7.8	13
[a]FJI-H8-Me	173.1	221.0	172.2	196.9	34.3	44.3	9.9	23
[a]JLU-MOF132	15.8	52.4	18	37.2	25.4	29.2	9.2	24
[a]Yb-pek-MOF-2	41.7	127.3	55	98.1	27.3	34	5.4	25
[a]Yb-pek-MOF-1	47.2	146.3	48.5	111.9	28	37.6	9	25
[a]CoV-$(CF_3)_2$bdc-tpt	65.9	79.1	60.5	68.5	26.2	36	10.1	26
[a]FJI-W9	66	83	68	76.5	20.9	38	20.5	27
[a]**fcu**-BPyDC-Yb	58.9	175	102.1	155.9	17.60	29.69	9.4	This work
[a]**fcu**-BPyDC-Y	72.0	209.5	120.3	186.7	20.58	32.48	9.1	This work

"a" indicates that the temperature is 298 K; "b" indicates that the temperature is 295 K.

8. High-Pressure Methane Sorption Measurements

High-pressure excess methane sorption isotherms were measured with an automatic volumetric sorption apparatus (BELSORP-HP) in the range of 0-80 bar. The bath temperature for CH_4 sorption measurements was controlled using a recirculating bath containing an ethylene glycol/H_2O mixture. Ultrahigh purity He was used to determine the dead space of the sample cell. The sorption data were corrected to give the final gravimetric excess sorption isotherm n_{ex} (P, T), by subtracting the background sorption measured with the empty sample cell using the same test parameters. The total sorption, which represents the real gas-storage performance of the porous material but cannot be directly measured, was calculated by (Eqn. (5)):

$$n_{tot}(P,T) = n_{tot}(P,T) + \rho_{gas}(P,T) \times V_P \qquad (5)$$

Where ρ_{gas} (P, T) is the density of bulk methane at pressure *P* and temperature *T*, and V_p is the pore volume of the porous material determined from N_2 adsorption isotherm at 77 K.

The isosteric enthalpy of adsorption, Q_{st} for methane was determined by fitting the adsorption isotherms at 273 and 298 K to the Dual-site Langmuir equation (Eqn. 3);

Using the Dual-site Langmuir fit, the isosteric heat of adsorption can be calculated for the material as a function of the total amount of methane adsorbed using the Clausius-Clapeyron relation (Eqn. (6)):

$$\frac{dlnp}{dT} = \frac{\Delta H}{nRT^2} = \frac{\Delta_r H_m}{RT^2} \qquad (6)$$

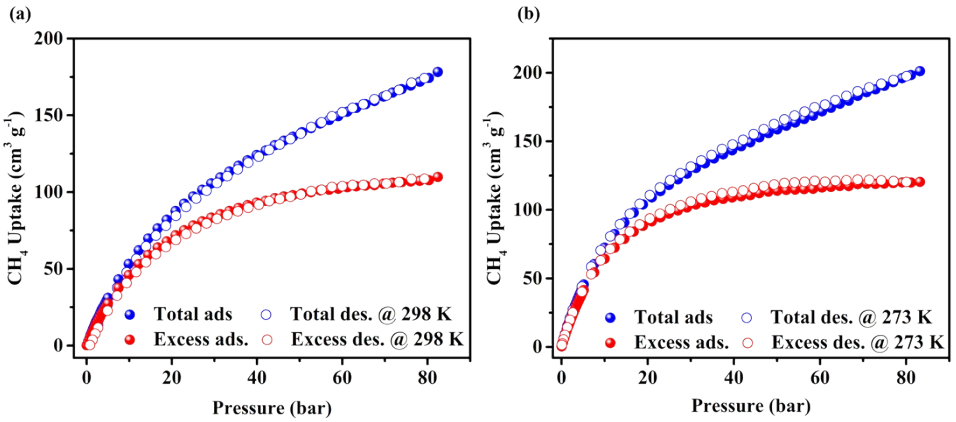

Fig. S14 High-pressure CH_4 sorption isotherms at (a) 298 K and (b) 273 K for **fcu**-BPyDC-Yb.

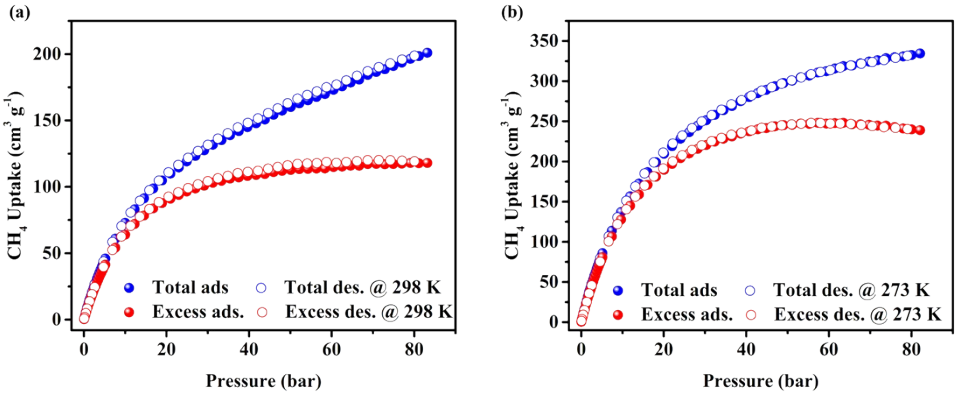

Fig. S15 High-pressure CH_4 sorption isotherms at (a) 298 K and (b) 273 K for **fcu**-BPyDC-Y.

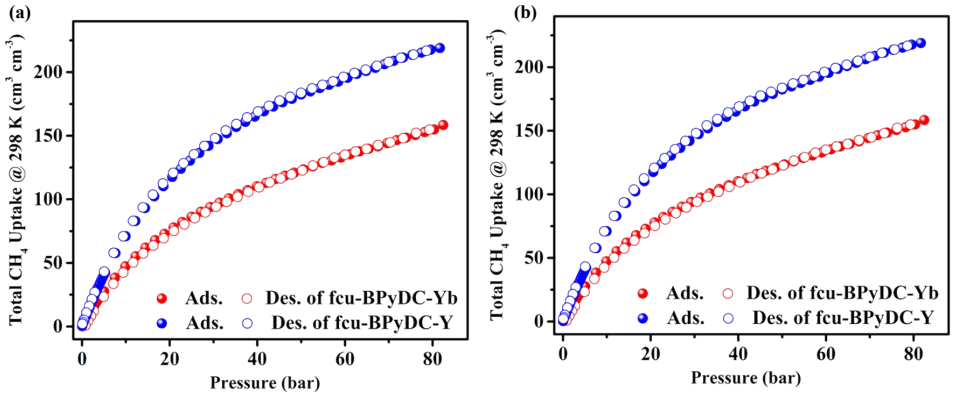

Fig. S16 The total CH_4 adsorption isotherms at 298 K (a) and 273 K (b) for **fcu**-BPyDC-Yb and **fcu**-BPyDC-Y, respectively.

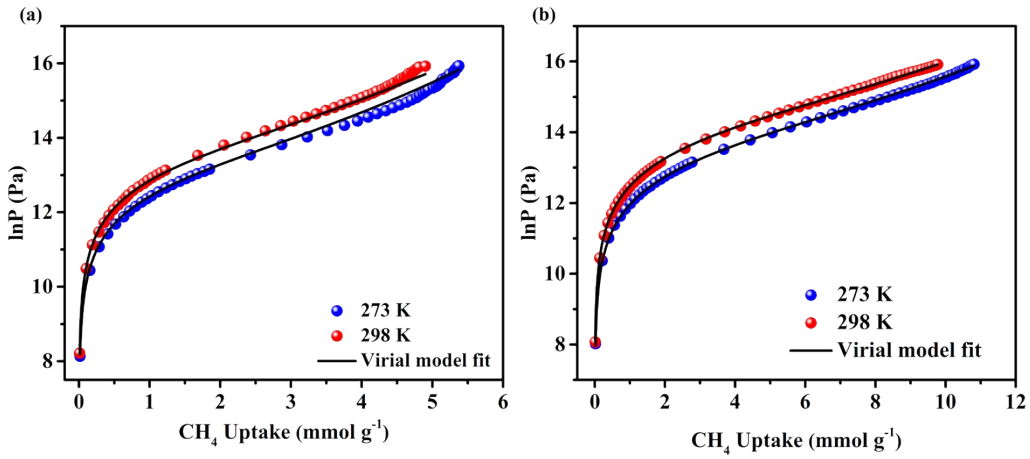

Fig. S17 Virial model fit (lines) of CH_4 adsorption isotherms (points) measured at 273 and 298 K for **fcu**-BPyDC-Yb (a) **fcu**-BPyDC-Y (b), respectively.

Table S5. The obtained Virial model fitting parameters for **fcu**-BPyDC-Yb

T (K)	a0	a1	a2	a3	b0	R^2
273	-1395.87877	7.00385	10.47632	0.95376	17.47038	0.99538
298	-1395.87877	7.00385	10.47632	0.95376	17.47038	0.99591

Table S6. The obtained Virial model fitting parameters for **fcu**-BPyDC-Y

T (K)	a0	a1	a2	a3	b0	R^2
273	-1736.32670	25.42417	-0.62401	0.19341	18.22314	0.99982
298	-1736.32670	25.42417	-0.62401	0.19341	18.22314	0.99986

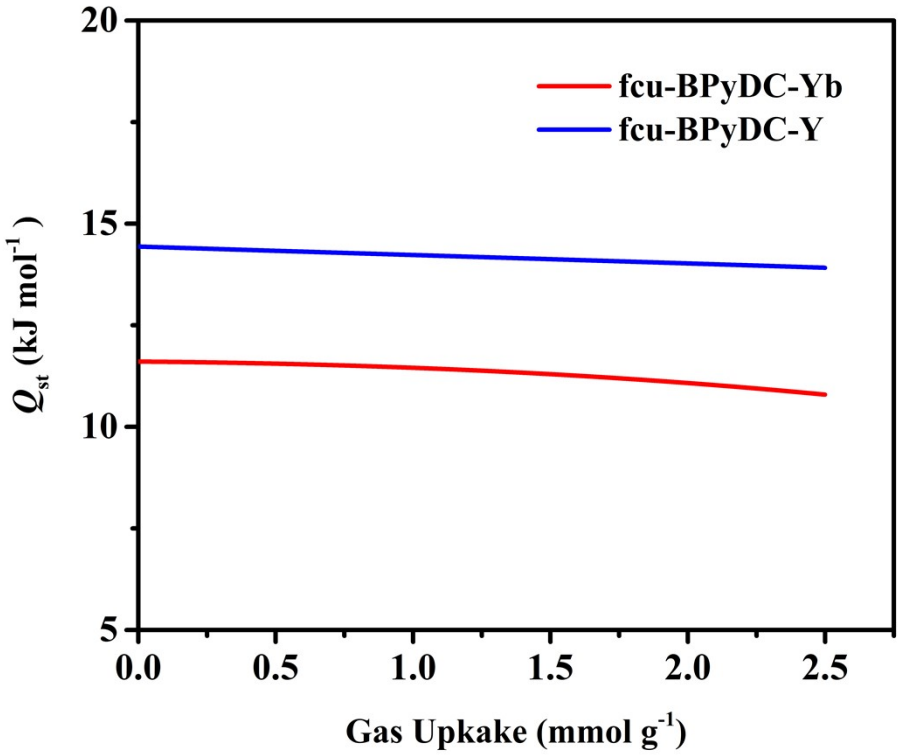

Fig. S18 Heats of CH_4 adsorption (Q_{st}) for **fcu**-BPyDC-Yb (red) and **fcu**-BPyDC-Y (blue), which were calculated from the dual-site Langmuir model fitting of adsorption isotherms at 273 and 298 K as a function of the total CH_4 uptake amount using the Clausius-Clapeyron equation (eqn (6)).

Table S7. The methane adsorption data summary of **fcu**-BPyDC-Yb.

Name	BET $m^2 g^{-1}$	V_p $cm^3 g^{-1}$	ρ g cm^{-3}	T(K)	Uptake $cm^3 g^{-1}$ 5/80 bar	Working Capacity $cm^3 g^{-1}$ 5-80 bar	Uptake g g^{-1} 5/80 bar	Working Capacity g g^{-1} 5-80 bar	Uptake $cm^3 cm^{-3}$ 5/80 bar	Working Capacity $cm^3 cm^{-3}$ 5-80 bar	Q_{st} (kJ mol^{-1})
fcu-BPyDC-Yb	2114	0.80	0.889	298	30/175	145	0.02/0.13	0.103	28/155	127	11.61
				273	44/197	153	0.03/0.14	0.109	29/175	146	

Table S8. The methane adsorption data summary of **fcu**-BPyDC-Y.

Name	BET $m^2 g^{-1}$	V_p $cm^3 g^{-1}$	ρ g cm^{-3}	T(K)	Uptake $cm^3 g^{-1}$ 5/80 bar	Working Capacity $cm^3 g^{-1}$ 5-80 bar	Uptake g g^{-1} 5/80 bar	Working Capacity g g^{-1} 5-80 bar	Uptake $cm^3 cm^{-3}$ 5/80 bar	Working Capacity $cm^3 cm^{-3}$ 5-80 bar	Q_{st} (kJ mol^{-1})
fcu-BPyDC-Y	2511	0.96	0.724	298	55/300	245	0.04/0.22	0.177	40/218	178	14.43
				273	83/333	250	0.06/0.24	0.180	61/241	180	

9. Single-Crystal X-ray Diffraction Studies

Single-crystal X-ray diffraction data for **fcu**-BPyDC-Yb was collected on a Bruker D8 venture diffractometer (Cu/$K\alpha$, λ = 1.54178 Å) at 173 K. Indexing was performed using APEX3 (Difference Vectors method).[28] Data integration and reduction were performed using SaintPlus 6.01. Absorption correction was performed by multiscan method implemented in SADABS.[29] Space group was determined using XPREP implemented in APEX3. These structures were solved by direct methods and refined with full-matrix least squares technique using the SHELXT[30] package or refined using SHELXL-2014 (full-matrix least-squares on F^2) contained in Olex2.[31] Non-hydrogen atoms were refined with anisotropic displacement parameters during the final cycles. Hydrogen atoms were located at geometrically calculated positions to their carrier atoms and refined with isotropic thermal parameters included in the final stage of the refinement. For this compound, the contributions of heavily disordered solvent molecules were treated as diffuse using Squeeze procedure implemented in Platon program.[32]

A summary of the crystallographic data is given in Table S9 CCDC **2417528** (**fcu**-BPyDC-Yb), contain the supplementary crystallographic data for this paper. These data can be obtained free of charge from the Cambridge Crystallographic Data Centre.

Table S9. Crystal data and refinement results for **fcu**-BPyDC-Yb

Identification code	**fcu**-BPyDC-Yb
Empirical formula	$C_{30}H_{12}F_4N_{12}O_{15}Yb_3$
Formula weight	1375.64
Temperature/K	173.00
Crystal system	Cubic
Space group	*Fm*-3*m*
Unit cell dimensions	a = 27.0155(3) Å
Volume/Å^3	19716.9(7)
Z	8
ρ_{calc}g/cm^3	0.927
μ/mm^{-1}	5.450
***F* (000)**	5136.0
Crystal size/mm^3	0.16 × 0.08 × 0.08
Radiation	CuK_α (λ = 1.54178)
2θ range for data collection/°	9.258 to 117.752
Index ranges	$-1 \le h \le 30$, $-16 \le k \le 26$, $-22 \le l \le 26$
Reflections collected	5827
Independent reflections	770
R_{int}	0.0276
Data/restraints/parameters	770/25/40
Goodness-of-fit on F^2	1.107
Final R indexes (I>2σ (I))	R_1 = 0.0455, wR_2 = 0.1282
Final R indexes (all data)	R_1 = 0.0493, wR_2 = 0.1317
Largest diff. peak/hole/e Å^{-3}	0.71/-1.13

10. Grand Canonical Monte Carlo (GCMC) Simulation.

Gas adsorption behavior on the MOFs were simulated by the GCMC method. All GCMC simulations were performed using the Sorption modules in Materials Studio. The Universal force field was used to describe interatomic interactions. The Ewald method was used to calculate the electrostatic energy.[33] The cutoff radius for van der Waals interactions is set at 18.5 Å, the equilibrium stride for each calculation cycle is 1×10^7, Use an adsorption model with a fixed adsorption pressure (density distribution) of 100 kPa and a fixed adsorption capacity (preferred adsorption sites) for simulation calculations.

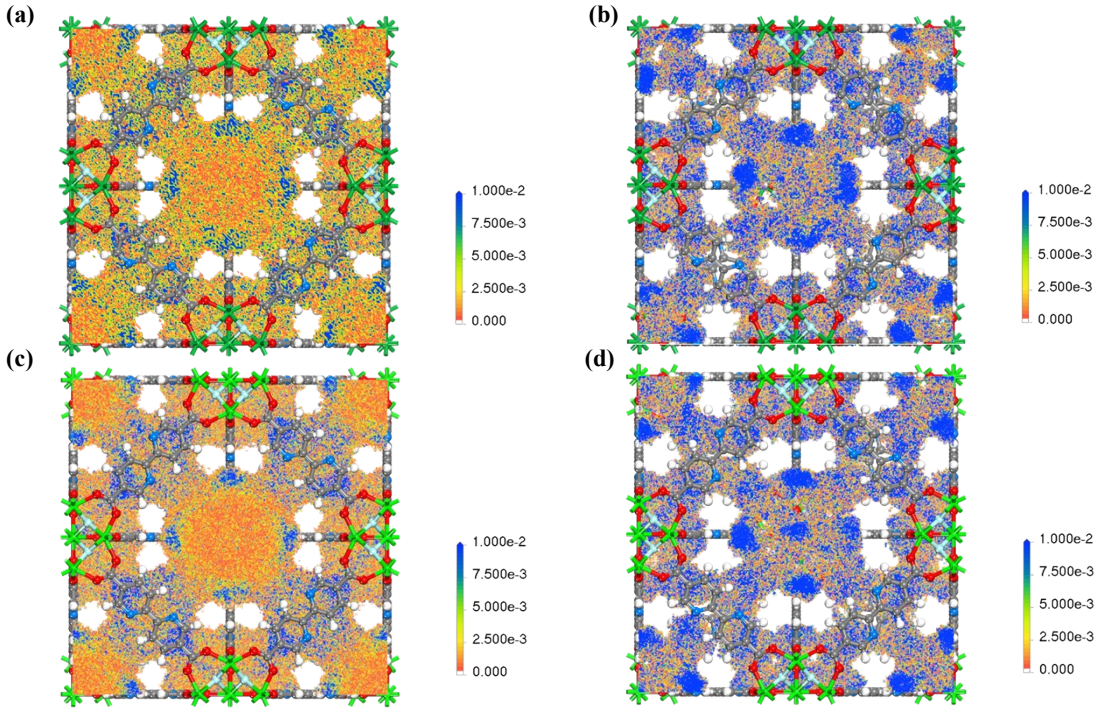

Fig. S19 C_2H_4 and C_3H_6 density distributions at 1 bar were within favorable adsorption sites of **fcu**-BPyDC-Yb (a and b) and **fcu**-BPyDC-Y (c and d), respectively.

11. References

1 E. Ning, L. Yang, B. Tu, Q. Pang, X. Li, H. Xu, Y. Qi and Q. Li, *J. Colloid Interface Sci.*, 2019, **552**, 372-377.

2 A. L. Myers and J. M. Prausnitz, *AlChE J.*, 1965, **11**, 121-127.

3 Y.-S. Bae, K. L. Mulfort, H. Frost, P. Ryan, S. Punnathanam, L. J. Broadbelt, J. T. Hupp and R. Q. Snurr, *Langmuir*, 2008, **24**, 8592-8598.

4 B. Mu, F. Li and K. S. Walton, *Chem. Commun.*, 2009, DOI: 10.1039/B819828D, 2493-2495.

5 L. Zhang, L.-N. Ma, G.-D. Wang, L. Hou, Z. Zhu and Y.-Y. Wang, *J. Mater. Chem. A*, 2023, **11**, 2343-2348.

6 W. Fan, Y. Wang, Q. Zhang, A. Kirchon, Z. Xiao, L. Zhang, F. Dai, R. Wang and D. Sun, *Chem. Eur. J.*, 2018, **24**, 2137-2143.

7 H. Fang, B. Zheng, Z.-H. Zhang, H.-X. Li, D.-X. Xue and J. Bai, *Angew. Chem. Int. Ed.*, 2021, **60**, 16521-16528.

8 C.-X. Chen, Z.-W. Wei, Q.-F. Qiu, Y.-Z. Fan, C.-C. Cao, H.-P. Wang, J.-J. Jiang, D. Fenske and C.-Y. Su, *Cryst. Growth Des.*, 2017, **17**, 1476-1479.

9 X. Liu, C. Hao, J. Li, Y. Wang, Y. Hou, X. Li, L. Zhao, H. Zhu and W. Guo, *Inorg. Chem. Front.*, 2018, **5**, 2898-2905.

10 X. Liu, W. Fan, M. Zhang, G. Li, H. Liu, D. Sun, L. Zhao, H. Zhu and W. Guo, *Mater. Chem. Front.*, 2018, **2**, 1146-1154.

11 S. Gao, C. G. Morris, Z. Lu, Y. Yan, H. G. W. Godfrey, C. Murray, C. C. Tang, K. M. Thomas, S. Yang and M. Schröder, *Chem. Mater.*, 2016, **28**, 2331-2340.

12 W. Fan, X. Wang, X. Zhang, X. Liu, Y. Wang, Z. Kang, F. Dai, B. Xu, R. Wang and D. Sun, *ACS Cent. Sci.*, 2019, **5**, 1261-1268.

13 X.-M. Liu, L.-H. Xie and Y. Wu, *Materials*, 2023, **16**, 154.

14 X. Wu, Z. Bao, B. Yuan, J. Wang, Y. Sun, H. Luo and S. Deng, *Microporous Mesoporous Mater.*, 2013, **180**, 114-122.

15 D. Geng, M. Zhang, X. Hang, W. Xie, Y. Qin, Q. Li, Y. Bi and Z. Zheng, *Dalton*

Trans., 2018, **47**, 9008-9013.

16 Y. Zhang, X.-Q. Meng, H.-J. Ding, X. Wang, M.-H. Yu, S.-M. Zhang, Z. Chang and X.-H. Bu, *ACS Appl. Mater. Interfaces*, 2019, **11**, 20995-21003.

17 G. Chang, M. Huang, Y. Su, H. Xing, B. Su, Z. Zhang, Q. Yang, Y. Yang, Q. Ren, Z. Bao and B. Chen, *Chem. Commun.*, 2015, **51**, 2859-2862.

18 G.-D. Wang, Y.-Z. Li, R. Krishna, W.-Y. Zhang, L. Hou, Y.-Y. Wang and Z. Zhu, *Angew. Chem. Int. Ed.*, 2024, **63**, e202319978.

19 G.-D. Wang, R. Krishna, Y.-Z. Li, Y.-Y. Ma, L. Hou, Y.-Y. Wang and Z. Zhu, *ACS Mater. Lett.*, 2023, **5**, 1091-1099.

20 G.-D. Wang, Y.-Z. Li, W.-J. Shi, L. Hou, Y.-Y. Wang and Z. Zhu, *Angew. Chem. Int. Ed.*, 2023, **62**, e202311654.

21 Y.-Z. Li, G.-D. Wang, R. Krishna, Q. Yin, D. Zhao, J. Qi, Y. Sui and L. Hou, *Chem. Eng. J.*, 2023, **466**, 143056.

22 G. Zhen, Y. Liu, Y. Zhou, Z. Ji, H. Li, S. Zou, W. Zhang, Y. Li, Y. Liu, C. Chen and M. Wu, *ACS Appl. Mater. Interfaces*, 2024, **16**, 1179-1186.

23 Z. Di, Z. Ji, C. Chen, R. Krishna, D. Yuan, M. Hong and M. Wu, *Chem. Eng. J.*, 2024, **493**, 152442.

24 D. Wang, Z. Shi, W. Li, G. Li, X. Liu and Y. Liu, *Chem. Eng. J.*, 2024, **498**, 155176.

25 W.-Q. Wei, X.-A. Guo, Z.-H. Zhang, Y.-F. Zhang and D.-X. Xue, *Inorg. Chem. Commun.*, 2021, **133**, 108896.

26 Y. Xiao, A. N. Hong, Y. Chen, H. Yang, Y. Wang, X. Bu and P. Feng, *Small*, 2023, **19**, 2205119.

27 H. Li, Y. Zhou, C. Chen, Y. Li, Z. Liu, M. Wu and M. Hong, *Inorg. Chem.*, 2024, **63**, 21548-21554.

28 Bruker APEX2; Bruker AXS, Inc.: Madison, WI, 2010.

29 G.M. Sheldrick, Sadabs, 1996.

30 G. Sheldrick, *Acta Crystallogr.* 2015, **71**, 3-8.

31 O.V. Dolomanov, L.J. Bourhis, R.J. Gildea, J.A.K. Howard, H. Puschmann, *J. Appl. Crystallogr.,* 2009, **42**, 339-341.

32 A.L. Spek, *J. Appl. Cryst.,* 2003, **36** 7-13.

33 L. Zhang, H. Chen, P. Liu, Y. Chen, Y. Liu, R.-B. Lin, X.-M. Chen, J. Li and L. Li, *J. Colloid Interface Sci.*, 2024, **656**, 538-544.